Int. J. Morphol.,
40(2):360-368, 2022.

Movable Surface Models of Hand Joints Using Visible Korean

Modelos de Superficies Móviles de Articulaciones de Manos Utilizando Visible Korean

Chung Yoh Kim & Jin Seo Park

KIM, C. Y. & PARK, J. S. Movable surface models of hand joints using Visible Korean. *Int. J. Morphol., 40(2)*:360-368, 2022.

SUMMARY: The human hand can make precise movements utilizing several joints of various articular types. To understand hand movements more accurately, it is essential to view the actual movements of bones and muscles considering the X, Y, and Z axes in the joints. This study aimed to investigate the joint movements in a hand using movable surface models, including these axes. These movable surface models of the hand will improve medical students' understanding of hand movements around the joints.To achieve this aim, 70 surface models were adopted from a Visible Korean model. Using Maya software, 20 virtual joints with X, Y, and Z axes included nine distal and proximal interphalangeal joints, five metacarpophalangeal joints, five carpometacarpal joints, and one wrist joint were created. Bone surface models were elaborately polished to maintain their original shape during movement. Muscle surface models were also processed to display the deformation of the muscle shape during movement. The surface models of the hand joints were moved by virtual control of the joints. We saved 87 movable surface models of the hand, including bones, muscles, and joint axes in stereolithography format, and compiled a Portable Document Format (PDF) file.Using the PDF file, the joint movements in a hand could be observed considering the X, Y, and Z axes alongside the stereoscopic shapes of the bones and muscles.These movable surface models of the hand will improve medical students' understanding of hand movements around the joints.

KEY WORDS: Hand Joints; Muscle Contraction; Muscle Relaxation; Three-Dimensional imaging,; Visible Human Projects.

INTRODUCTION

In wrist, intercarpal, intermetacarpal, carpometacarpal, metacarpophalangeal, and interphalangeal joints of human hand, there are 34 joints composed of four different types of synovial joints (plane, hinge, condyloid, and saddle types). By virtue of these features of the joints, the human hand can perform precise movements (Moore *et al*., 2018a).

On the other hand, it is not easy for medical students to understand the movements of a hand due to the different types of synovial joints with different articular surfaces. In contrast to the other fingers, the thumb is rotated about 90 degrees medially, and the shape of the first carpometacarpal joint is a saddle joint, which is unlike any other carpometacarpal (Moore *et al*., 2018a). To exactly understand the movements around the joints of the hand, it was necessary to observe the realistic movements of the bones and muscles in the hand, considering X, Y, and Z axes of the joints.

Unfortunately, these movements and the relationships between each different structure in the joints of the hand could not be shown stereoscopically in anatomy textbooks. Moreover, none of the anatomy textbooks described the joints in terms of their X, Y, and Z axes. Although the students can move hand of a cadaver, it was difficult to observe the inner structures without damaging the external structures (Ling & Kumar, 2008), and it was impossible to show realistic movements of the bones and muscles with axes of the joints. Finally, the existed three-dimensional (3D) models could aid the learning of the hand anatomy but they did not explain the joint movements in terms of the joint axes (Lewis *et al*., 2014; Zilverschoon *et al*., 2017, 2019).

This study aimed to investigate the movements in the joints of a hand using movable surface models, including the X, Y, and Z axes. We used surface models from a Visible Korean (Shin *et al*., 2012a), which were moved on the X, Y,

Department of Anatomy, Dongguk University School of Medicine, Gyeongju, Korea.
FUNDING: This research was supported by Basic Science Research Program through the National Research Foundation of Korea (NRF) funded by the Ministry of Education (NRF-2021R1F1A1063044).

Received: 31-08-2021 Accepted: 12-10-2021

and Z axes of the joints to simulate the movements of the bones and muscles of the hand.

MATERIAL AND METHOD

We produced 642 surface models of the whole body from the sectioned images of a Visible Korean (Park *et al*., 2005). From these, we selected the surface models of 40 muscles and 30 bones of the right hand (Table I). From the 34 joints (9 interphalangeal, 5 metacarpophalangeal, 4 intermetacarpal, 5 carpometacarpal, 10 intercarpal, and 1 wrist joints) in a real hand, we selected only 20 joints (9 interphalangeal, 5 metacarpophalangeal, 5 carpometacarpal, and 1 wrist joints) to construct movable surface models of the hand. These 20 joints were selected because they allowed prominent movements (Moore *et al*., 2018a).

In the surface models of thumb, the articular surfaces of each bone were identical to those of a real thumb because the thumb bones were segmented perfectly in the sectioned images (Shin *et al*., 2012c). However, the surface models of the phalanges and the metacarpal bones from the second to fifth were not identical to real hand, and they needed to be trimmed. In Maya version 2018 (Autodesk, Inc., San Rafael, CA), the distal and proximal articular surfaces of the distal, middle, and proximal phalanges and of the metacarpal bones were trimmed to create convex and concave articular surfaces using 'Move, Smooth, Relax, Grab, and Flatten' tools to make them more similar to the those of a living body (Kim *et al*., 2021b).

After trimming the articular surfaces in the bone surface models, 20 virtual joints were inserted to create nine distal and proximal interphalangeal joints, five metacarpophalangeal joints, five carpometacarpal joints, and one wrist joint using the 'Create Joints' tool in Maya. Next, the surface models of the carpal bones, metacarpals, and phalanges were bound to the corresponding virtual joints using the 'Bind Skin' tool. To prevent deformation of the bone surface models during movement, the 'Paint Skin Weight' tool was used. To explain the movements, we used the 'Cylinder' tool to create the X, Y, and Z axes of the joints, and these were placed into 17 virtual joints (nine interphalangeal, five metacarpophalangeal, two carpometacarpal, and one wrist joints). The X, Y, and Z axes represent the medial-lateral, anterior-posterior, and superior-inferior axes of the hand, respectively (Kim *et al*., 2021a).

We used Ziva VFX version 1.3 (Ziva Dynamics Inc., Vancouver, Canada), a Maya plug-in, to give realistic movements to the surface models. The bone surface models were processed using the 'Bone' tool to act as attachment points for the muscle origins and insertions. The muscle surface models were processed using the 'Tissue' tool to contract and expand like real muscles. After applying this tool to each muscle surface, parts of the muscle meshes were selected to be attached to the bones using the 'Attachment-fixed type' tool to act as origins and insertions, like real muscles. To avoid overlapping of the muscle surface models during movements, overlapping parts of muscles were selected using the 'Select Vertices' tool and processed with the 'Attachment-sliding type' tool (Kim *et al*., 2021a).

After processing the surface models for bones and muscles, the virtual joints were controlled using Maya to simulate movements in the hand joints. The original position of the surface models were recorded in the first time-frame slider. The anatomical position of the surface models were recorded in the middle, and all flexion positions of the wrist joint of the surface models were recorded in the last time-frame slider. We examined the movements of muscles and bones from the anatomical position to the flexion position in the wrist joint using the 'Play' tool, and differences between the surface models and real anatomical movements were modified. The surface models in the anatomical position and the last frames were saved in stereolithography (STL) (Kim *et al*., 2021a). Movements of other joints of the hand were processed in the same way. Consecutively, 58 movements in 20 virtual joints were saved in Maya Binary (MB) format.

In total, we uploaded 87 STL files of 58 movements to Deep Exploration 6.3 (SAP America, Inc., Newton Square, PA, USA) and classified them into each movement. The classified STL files were compiled into one portable document format (PDF) file to make it readily accessible to general personal computer environments. In Adobe Acrobat (Adobe Systems, Inc., San Jose, CA, USA), the movements of each joint were bookmarked using the 'Create View' tool (Shin *et al*., 2012b).

RESULTS

The movable surface models of 87 structures (30 bones, 40 muscles, and 17 joint axes) (Table I) and 58 movements in 20 virtual joints [9 distal and proximal interphalangeal joints (Fig. 1), 5 metacarpophalangeal joints (Fig. 2), 5 carpometacarpal joints (Fig. 3), and 1 wrist joint (Fig. 4)] were produced. All structures and all movements of the movable surface models were put into a MB file (file size, 11.2 megabytes). Each structure and each movements of the models were put into 1,249 STL files (total file size,

46.2 megabytes).In the PDF file (file size, 8.2 megabytes), the surface models of 87 structures (Table I) could be browsed using free viewpoints. In the bookmark window of the PDF file, the 58 movements of the muscles and bones could be observed in real-time by clicking on each movement folder (Figs. 1 to 4). Furthermore, 58 movements of bones caused by muscles located at the joints could be precisely scrutinized on the X, Y, and Z axes in four types of synovial joints using the PDF file, as described below.

Interphalangeal joints. The interphalangeal joints of the second to fifth digits permitted two movements (flexion and extension) in the X-axis and the YZ plane (sagittal) because the joints were the hinge type. By contracting the flexor digitorum superficialis and flexor digitorum profundus, the distal and middle phalanges were pulled to the proximal phalange. Consequently, anterior rotation occurred in the X-axis and the anterior YZ plane of each interphalangeal joint (flexion) (Fig. 1A; Table I). Posterior rotation occurred in the X-axis and the posterior YZ plane of the joints (extension) by contraction of the extensor digitorum, extensor digiti minimi, and extensor indicis (Fig. 1B; Table I). Hyperextension did not occur in the proximal interphalangeal joints because of extensor expansion, similar to thick ligaments, on the posterior surfaces of the phalanges. However, a small degree of hyperextension occurred in the distal interphalangeal joints from the second to fifth digits because the distal parts of the extensor expansion were thinner than the proximal parts (Fig. 1C; Table I).

In the interphalangeal joint of thumb, flexion and extension occurred as for other joints, but the movements occurred in the Y-axis and the XZ plane (coronal plane) instead. In general, full hyperextension of this joint is not possible, however, some people have a 'hitchhiker's thumb,' which enables hyperextension of this joint, unlike other interphalangeal joints (Glass & Kistler, 1953; Onyije *et al*., 2012). Therefore, we created surface models of the 'hitchhiker's thumb' (Fig. 1F; Table I).

Metacarpophalangeal joints. In the metacarpophalangeal joints, the proximal end of the proximal phalanges and the distal ends of the metacarpal bones were oval convex and oval concave, respectively. Due to the oval shape, known as a condyloid-type, the joints only allowed flexion-extension and abduction-adduction, unlike the saddletype.

Metacarpophalangeal joints from the second to fifth digits permitted two types of movement (flexion and extension) in the X-axis and the YZ plane (sagittal plane)

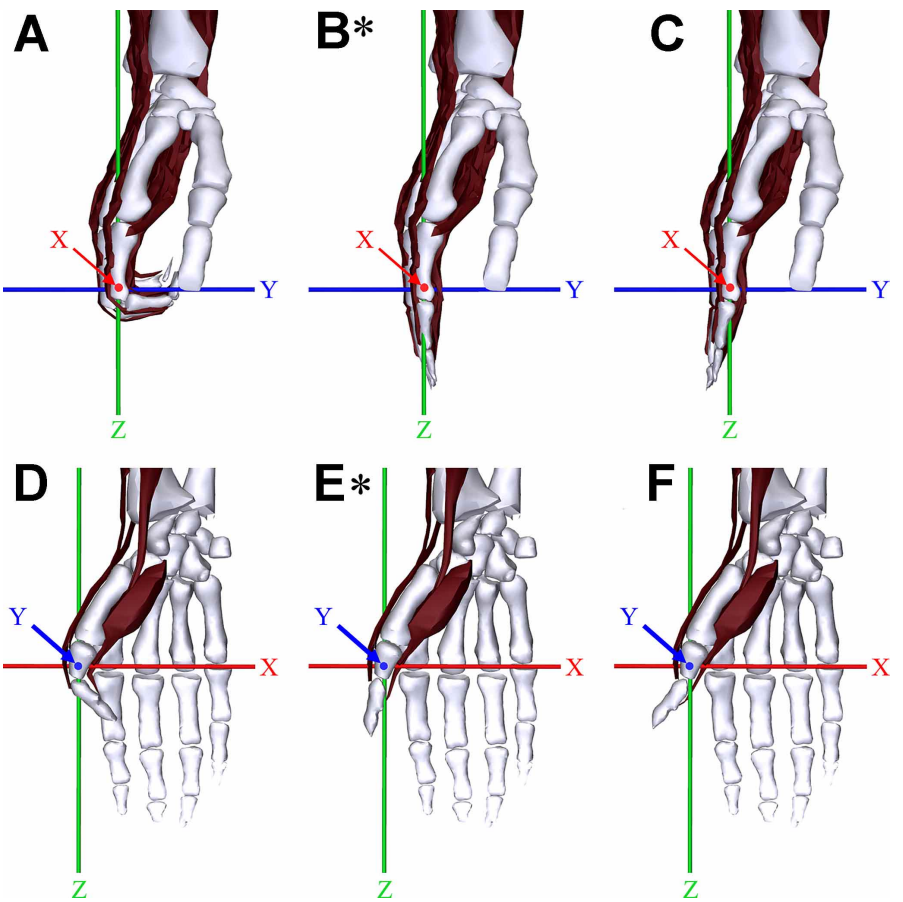

Fig. 1. Twenty-seven movements of the interphalangeal joints (hinge type) (A-C, lateral view; D-F, anterior view; *Anatomical position). A, Flexion of the second interphalangeal proximal joint is caused by anterior rotation in the X-axis; B, extension and C, hyperextension of the second proximal interphalangeal joint are caused by posterior rotation in the X-axis; D, flexion of the first distal interphalangeal joint is caused by medial rotation in the Y-axis; E, extension and F, hyperextension of the first distal interphalangeal joint are caused by lateral rotation in the Y-axis.

Table I. Seventy selected structures in surface models constructed from the Visible Korean model

System	Structures
Skeletal	Humerus, radius, ulna, scaphoid, lunate, triquetrum, pisiform, trapezium, trapezoid, capitate, hamate, first - fifth metacarpals, first - fifth proximal phalanges, second - fifth middle phalanges, first - fifth distal phalanges
Muscular	Deltoid, Supraspinatus, Infraspinatus, Teres minor, Teres major, Subscapularis, Biceps brachii, Coracobrachialis, Brachialis, Triceps brachii, Anconeus, Pronator teres, flexor carpi radialis[d, e, g], palmaris longus[d, e], flexor carpi ulnaris[d, e, h], flexor digitorum superficialis[a, b, e], flexor digitorum profundus[a, e], flexor pollicis longus[a, b, c, e], pronator quadratus, brachioradialis, extensor carpi radialis longus[d, f, g], extensor carpi radialis brevis[d, f, g], extensor digitorum[a, b, f], extensor digiti minimi[a, b, f], extensor carpi ulnaris[d, f, h], supinator, abductor pollicis longus[c, g], extensor pollicis brevis[a, b, c, f], extensor pollicis longus[a, b, c, f], extensor indicis[a, b, f], abductor pollicis brevis[c, g], flexor pollicis brevis[a, b, c, e], opponens pollicis[c, e, g], adductor pollicis[c, h], abductor digiti minimi[b, g], flexor digiti minimi brevis[b, e], opponens digiti minimi[c, g], lumbrical muscle[a, b, e, f], dorsal interossei[b, g], palmar interossei[b, h]

[a]Distal and proximal interphalangeal joints (Hinge type); [b]Metacarpophalangeal joints (Condyloid type); [c]First carpometacarpal joint (Saddle type); [d]Wrist joint (Condyloid type); [e]Flexion; [f]Extension; [g]Abduction; [h]Adduction.

because the joints were the condyloid type. As with the interphalangeal joints, contraction of the flexor digitorum superficialis and flexor digitorum profundus resulted in anterior rotation in the X-axis and the YZ plane of each metacarpophalangeal joint (flexion) (Fig. 2A; Table I). Consequently, the phalanges were pulled towards the metacarpal bones. By contracting the extensor muscles, posterior rotation occurred in the X-axis and the YZ plane (extension) (Fig. 2B; Table I).

The metacarpophalangeal joints of the second to fifth digits permitted two types of movement (abduction and adduction) in the Y-axis and the XZ plane because the joints were the condyloid type. By contracting the dorsal interossei, lateral and medial rotations occurred in the Y-axis and the XZ plane of the second metacarpophalangeal joint and the fourth and fifth metacarpophalangeal joints, respectively. Consequently, the second, fourth, and fifth phalanges were spread, centering on the third metacarpophalangeal phalange (abduction) (Fig. 2C; Table I). By contracting the palmar interossei, medial and lateral rotations occurred in the Y-axis and the XZ plane of the second metacarpophalangeal joint and the fourth and fifth metacarpophalangeal joints, respectively (adduction) (Fig. 2D; Table I). Consequently, the phalanges were gathered, centering on the third metacarpophalangeal phalange. However, the third phalanx did not rotate on any axis because both the dorsal and palmar interossei were attached along the bilateral sides of the third phalanx (Figs. 2C and D).

The metacarpophalangeal joint of the thumb permitted only medial (flexion) and lateral (extension) rotations in the Y-axis and the XZ plane by contracting the flexor pollicis muscles and extensor pollicis muscles (Figs. 2E and F; Table I). Although the metacarpophalangeal joint of the thumb was a condyloid joint, the abduction and adduction movements are significantly less than those of the other metacarpophalangeal joints (Patel *et al*., 2010).

Carpometacarpal joint. The carpometacarpal joints of the second and third digits permit only slight movements because of the planetype joints (Batmanabane & Malathi, 1985). Therefore, the movements were not included in the movable surface models.

The carpometacarpal joint of the thumb was the only saddle joint in a hand. By contracting the flexor pollicis longus and brevis muscles, the first metacarpal bone was pulled towards the trapezium, causing medial rotation in the Y-axis and the XZ plane (flexion) (Fig. 3A; Table I). By contracting the extensor pollicis longus and brevis muscles, lateral rotation occurred in the Y-axis and the XZ plane (extension or hyperextension) (Figs. 3B and C; Table I).

By contracting the abductor pollicis longus and abductor pollicis brevis muscles, the first metacarpal bone was pulled away from the second metacarpal bone, causing anterior rotation in the X-axis and the YZ plane in the carpometacarpal joint (abduction) (Fig. 3D; Table I). When the adductor pollicis was contracted, the first metacarpal bone was pulled towards the second metacarpal bone, causing posterior rotation in the X-axis and the YZ plane in the carpometacarpal joint (adduction) (Fig. 3E; Table I).

Unusual movements of opposition and reposition occurred in the carpometacarpal joint of the thumb and the metacarpophalangeal joint of the fifth phalanx. Contraction of the opponens pollicis pulled the first metacarpal bone to the center of the palm, causing anterior rotation in the X-axis and the YZ plane (abduction) and medial rotation in the Y-axis and the XZ plane (flexion) (Fig. 3F). Simultaneously, in the fifth metacarpal joint, contraction

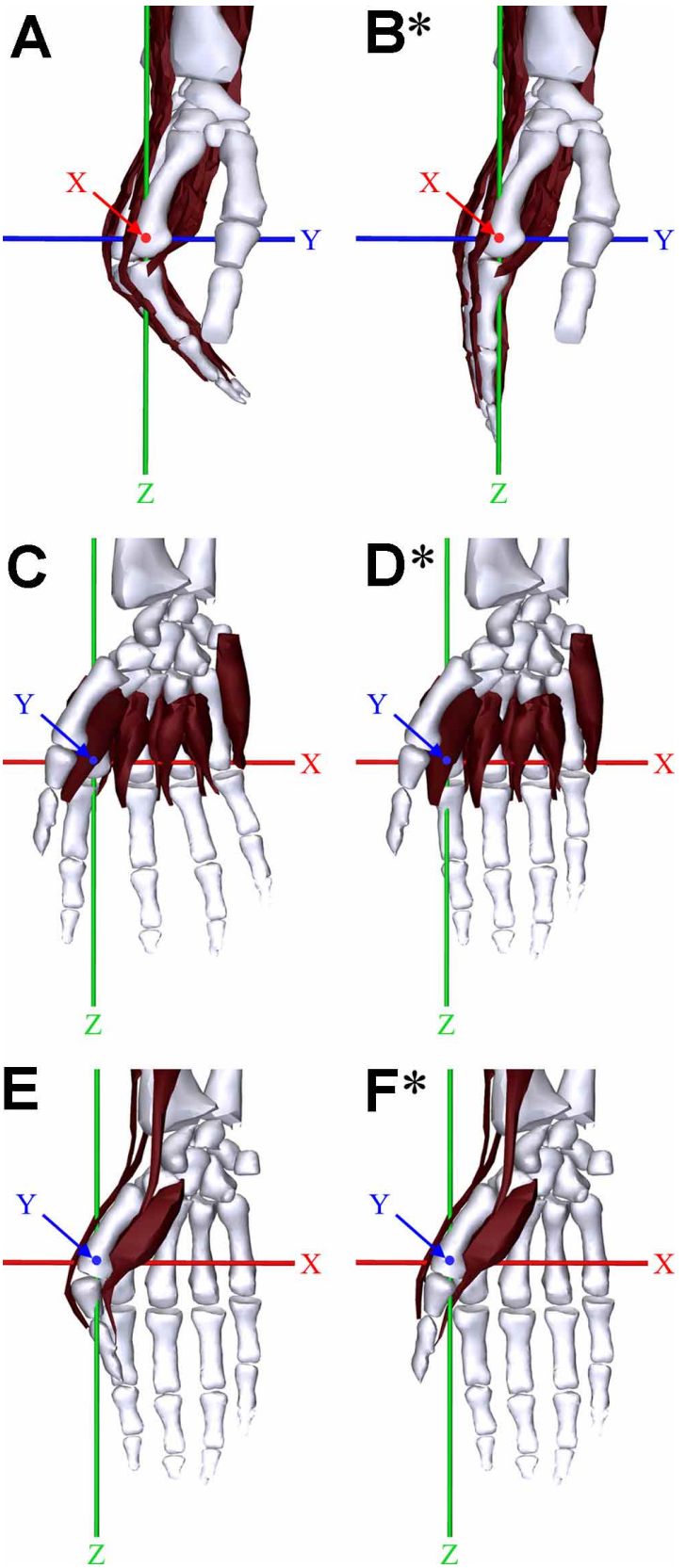

of the opponens digiti minimi pulled the fifth metacarpal bone to the center of the palm, causing anterior rotation in the X-axis and the YZ plane (flexion) and lateral rotation in the Y-axis and the XZ plane (adduction) (Fig. 3H). Relaxation of these muscles returned each digit to the anatomical position (reposition) (Figs. 3G and I).

The thumb was rotated approximately 90 degrees to the other digits. The start point of this rotation was the carpometacarpal joint of the thumb which was rotated approximately 45 degrees in the Z-axis and the XY plane (horizontal plane) (Figs. 3B and E), and the endpoint was the metacarpophalangeal joint which was rotated approximately 90 degrees in the Z-axis (Fig. 2F). This was confirmed by the movement and the shape of the head of the metacarpal bone in the thumb, compared to the other metacarpal bones. For this reason, flexion-extension of the thumb occurred in the Y-axis in the metacarpophalangeal joint (Figs. 2E and F), whereas flexion-extension of the second to fifth digits occurred in the X-axes in the metacarpophalangeal joints (Figs. 2A and B).

Wrist joint. In the wrist joint, the proximal ends of the carpal bones (except for the pisiform and distal end of radius) were convex and concave, respectively. Due to their uneven condyloidtype, the joints only allowed flexion-extension and abduction-adduction (Fig. 4).

Contracting the flexor muscles of the forearm pulled the hand toward the forearm, and anterior rotation occurred in the X-axis and the YZ plane of the wrist joint (flexion) (Fig. 4A; Table I). By contrast, contracting the extensor muscles of the forearm resulted in posterior rotation in the X-axis and the YZ plane (extension or hyperextension) (Figs. 4B and C; Table I).

Fig. 2. Sixteen movements of the metacarpophalangeal joints (condyloid type) (A-B, lateral view; C-F, anterior view; *Anatomical position). A, Flexion of the second metacarpophalangeal joint is caused by anterior rotation in the X-axis; B, extension of the second metacarpophalangeal joint is caused by posterior rotation in the X-axis; C, abduction of the second metacarpophalangeal joint is caused by lateral rotation in the Y-axis; D, adduction of the second metacarpophalangeal joint is caused by medial rotation in the Y-axis; E, flexion of the first metacarpophalangeal joint is caused by medial rotation in the Y-axis; F, extension of the first metacarpophalangeal joint is caused by lateral rotation in the Y-axis.

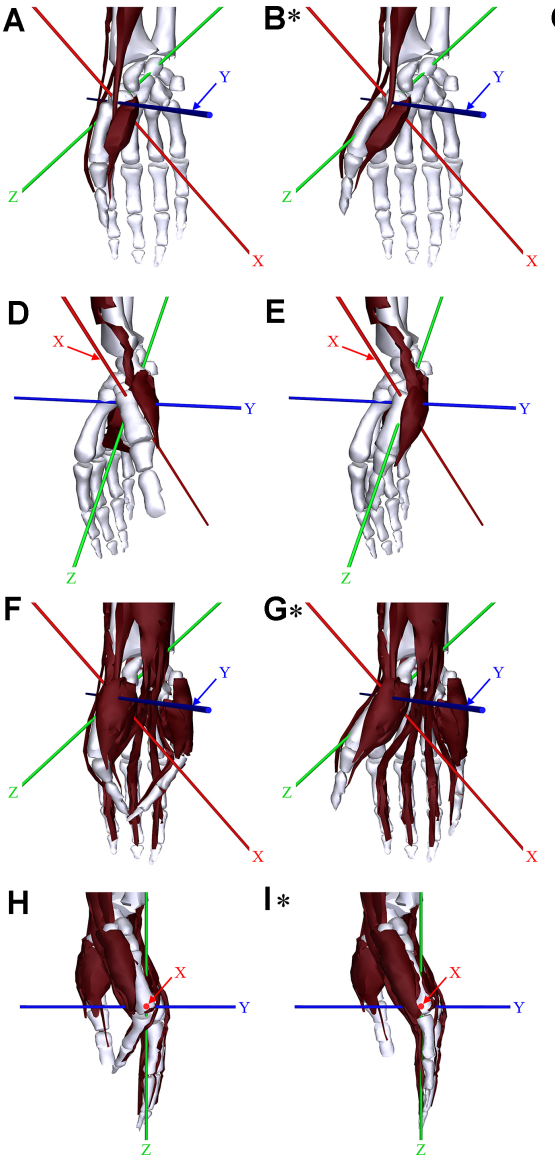

Fig. 3. Nine movements of the first carpometacarpal joint (saddle type) and fifth metacarpophalangeal joint (condyloid type) (A-C, F-G, anterior view; D-E, lateral view; H-I, medial view; *Anatomical position). A, Flexion of the first carpometacarpal joint is caused by anterolateral rotation in the Y-axis; B ,extension and C, hyperextension of the first carpometacarpal joint is caused by posteromedial rotation in the Y-axis; D, abduction of the first carpometacarpal joint is caused by anterior rotation in the X-axis; E, adduction of the first carpometacarpal joint is caused by posterior in the X-axis; F, opposition of the first carpometacarpal joint is caused by anterior rotation in the X-axis and medial rotation in the Y-axis; G, reposition of the first carpometacarpal joint is caused by posterior rotation in the X-axis and lateral rotation in the Y-axis; H, opposition of the fifth metacarpophalangeal joint is caused by anterior rotation in the X-axis and lateral rotation in the Y-axis; I, reposition of the fifth metacarpophalangeal joint is caused by posterior rotation in the X-axis and lateral rotation in the Y-axis.

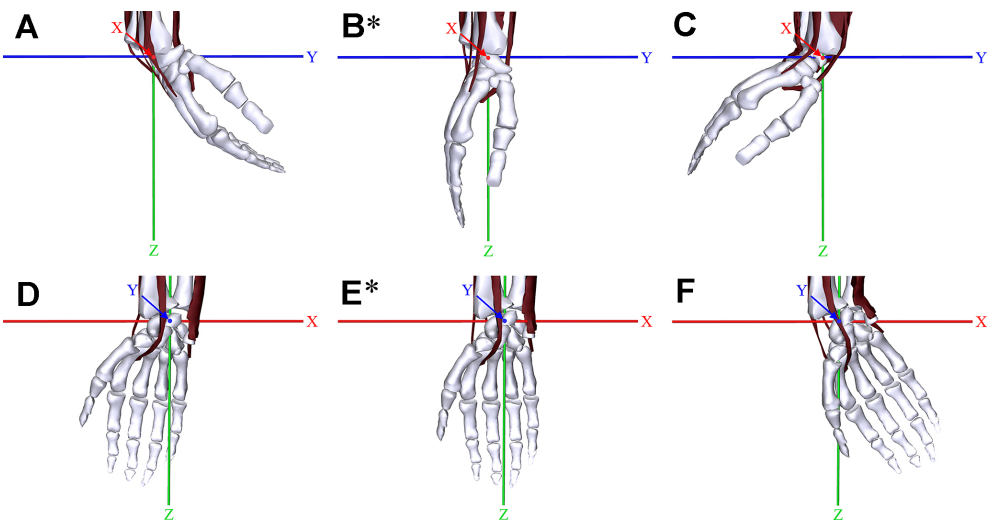

Fig. 4. Six movements of the wrist joint (condyloid type) (A-C, lateral view; D-F, anterior view; *Anatomical position). A, Flexion of the wrist joint is caused by anterior rotation in the X-axis of the wrist joint; B, extension and C, hyperextension of the wrist joint are caused by posterior rotation in the X-axis;D, abduction of the wrist joint is caused by lateral rotation in the Y-axis; E, and F, adduction of the wrist joint is caused by medial rotation in the-axis.

Contraction of both the flexor and extensor carpi radialis muscles rotated the hand laterally in the Y-axis and the XZ plane of the wrist joint (abduction) (Fig. 4D; Table I). However, contracting the flexor and extensor carpi ulnaris muscles (adduction) resulted in medial rotationin the Y-axis and the XZ plane (extension) (Fig. 4F; Table I). The motion range of adduction of the hand is wider than the range of abduction (Figs. 4D and F) because of the smaller styloid process of the ulna compared to the radius.

Other joints. The intercarpal joints, intermetacarpal joints, and carpometacarpal joints of the second and fifth digits were planetype that permits only gliding or sliding movements of the bones. These movements were not prominent compared to other joints (Moore *et al*., 2018a). Therefore, the movements of the joints were not constructed in the movable surface models.

DISCUSSION

To make surface models move realistically, there was a need for axes in the joints and realistic articular surfaces, and therefore we tried as follows for the realism.

The positions of the axes in the joints had to be determined. The essential factors in determining the positions of the axes were the shapes of the articular surfaces of each bone. Therefore, first, we trimmed the articular surfaces of the bone surface models to resemble the convex and concave articular surfaces of the living body as much as possible. Next, the axes of the virtual joints were pinned to the midpoints at the heads of bones with convex surfaces. Consequently, in the movable surface models, each bone with a convex surface became the axis, and each bone with a concave surface rotated (Fig. 5). One and two axes in the joints were required for bone rotation in hinge-type, and in condyloid-type and saddle-type joints, respectively (Figs. 1 to 3).

Furthermore, we also considered movement restriction due to the ligaments. Although we did not construct a ligament surface model in this study, the restrictive function of ligaments was applied in the movable surface models. Consequently, in the movable surface models, bones with one and two axes were only rotated in two (flexion and extension) (Fig. 1) and four (flexion, extension, abduction, and adduction) (Figs. 2 to 4) directions, respectively.

We realized three interesting features of the movements while we constructed the movable surface models of the hand.

First, in humans, why are all of the interphalangeal joints a hinge-type when condyloid or saddle joints in the interphalangeal joints would be more advantageous for free movement of the fingers? This can be explained in an evolutionary context, as all tetrapod animals need to run quickly to catch food or avoid predation. Therefore, they only need one-way propulsion to enable them to run. The hinge-type joints permit only one-way movement in one axis of rotation, and the flexor muscles of the hand provide the power for propulsion of the palm side of the hinge-type joint (Peters, 2000). In humans, although the joints and muscles are not used for running, the joints are a hinge-type because they are used to grip objects (Figs. 1A, B and C).

Second, a saddle-type joint rather than a condyloid-type joint at the first carpometacarpal is helpful in a hand. Due to orthograde walking, human hands have been freed and are deployed to perform other tasks, such as gripping objects. To grip an object firmly, the thumb needs rotary movements (circumduction and opposition) on two axes at the joint. Although both condyloid and saddle types of joints have two axes, the saddle-type makes rotary motions more freely than the condyloid-type because the articular surface of the condyloid-type is oval (Moore *et al*., 2018b). For this reason, the articular surfaces of the movable surface models were made to resemble the real surfaces as closely as possible (Fig. 5).

Finally, we carefully considered that the first metacarpal bone seems to be a proximal phalanx for the following reasons. First, in the movable surface models and the sectioned images (Park *et al*.), the shape of the first metacarpal bone was similar to the second to fifth proximal phalanges. In addition, the first proximal phalanx and the second to fifth middle phalanges were similar, in terms of length assessment (Figs. 1 to 5) (Pazzaglia *et al*., 2018). Second, there were similarities in terms of the distribution of the epiphyseal ossification centers and differential proximal-distal growth rates (Pazzaglia *et al*.). Third, anatomically, abduction and adduction movements in the first metacarpophalangeal joint, are restricted by collateral ligaments like interphalangeal joints, unlike other metacarpophalangeal joints despite the first metacarpophalangeal joint being the condyloid type (Moore *et al*., 2018b). In future work, we will aim to identify similarities from many computed tomography and magnetic resonance images to solve these issues.

Movable surface models of the hand were clearly displayed thanks to the segmented images from the sectioned images of the Visible Korean and the 3D motion tools of Maya and Ziva. The movable surface models could

realistically display various articular surfaces of several joints (Fig. 5) and showed the movements of bones by rotation in different axes in the joints of the hand (Figs. 1 to 5). We believe that the movable surface models described in this study will help medical students understand the exact the movements of the joints of the hand. In the future, surface models of other joints in the human body will be made movable using the methods developed in this study. The all data of this study are distributed freely on the website (anatomy.dongguk.ac.kr/hand). In the website, the movements of the hand joints can be displayed in real time on YouTubeTM.

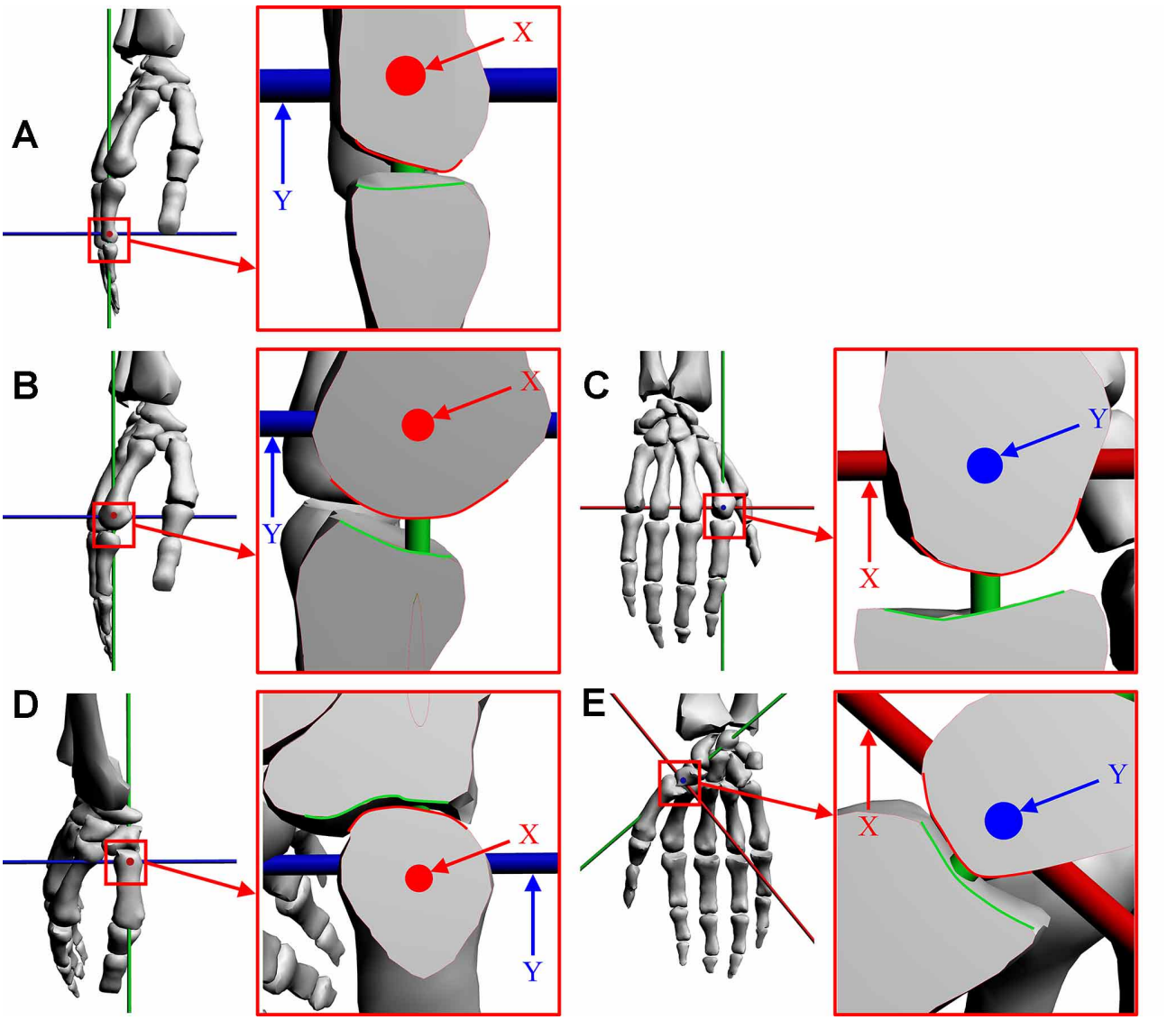

Fig. 5. Movements of bones with convex and concave articular surfaces in the axes of hinge-, condyloid-, and saddle-type joints (A, B, D, lateral view; C, posterior view; E, anterior view). A, In the hinge-type interphalangeal joint, the second middle phalanx of the concave surface head (green line) rotated anteriorly (flexion) and posteriorly (extension) in the X-axis (red point) in the second proximal phalanx of the convex surface head. In the condyloid-type metacarpophalangeal joint, the second proximal phalanx of the concave surface head (green line) rotated B, anteriorly (flexion) and posteriorly (extension) in the X-axis (red point) in the second metacarpal bone of the convex surface head and C, rotated anteriorly (abduction) and posteriorly (adduction) in the Y-axis (blue point) in second metacarpal bone of convex surface head. In the first saddle-type carpometacarpal joint, D, the first metacarpal bone of the convex surface head (red line) rotated anteriorly (abduction) and posteriorly (adduction) in the-X axis (red point) on the same first metacarpal bone of the concave surface head and E, the first metacarpal bone of the concave surface head (green line) rotated medially (flexion) and laterally (extension) in the Y-axis (blue point) in the trapezium of the convex surface head. (D) Except for the first metacarpal bone with both a convex surface head and an X-axis, (A, B, C, E) the bones of the concave surface head are rotated and an axis is located in the bones of the convex surface head.

ACKNOWLEDGMENTS

This research was supported by Basic Science Research Program through the National Research Foundation of Korea (NRF) funded by the Ministry of Education (NRF-2021R1F1A1063044).

FUNDING. This research was supported by Basic Science Research Program through the National Research Foundation of Korea (NRF) funded by the Ministry of Education (NRF-2021R1F1A1063044).

KIM, C. Y. & PARK, J. S. Modelos de superficies móviles de articulaciones de manos utilizando Visible Korean. *Int. J. Morphol., 40(2)*:360-368, 2022.

RESUMEN: La mano humana puede realizar movimientos precisos utilizando varias articulaciones de diferentes tipos articulares. Para comprender los movimientos de las manos con mayor precisión, es esencial ver los movimientos reales de los huesos y los músculos considerando los ejes X, Y y Z de las articulaciones. Este estudio tuvo como objetivo investigar los movimientos articulares en una mano utilizando modelos de superficies móviles, incluidos estos ejes. Estos modelos de superficie móvil de la mano mejorarán la comprensión de los estudiantes de medicina de los movimientos de la mano alrededor de las articulaciones. Para lograr este objetivo, se adoptaron 70 modelos de superficie de un modelo coreano visible. Con el software Maya, se crearon 20 articulaciones virtuales con ejes X, Y y Z que incluyeron nueve articulaciones interfalángicas distales y proximales, cinco articulaciones metacarpofalángicas, cinco articulaciones carpometacarpianas y una articulación de muñeca. Los modelos de superficie ósea se pulieron minuciosamente para mantener su forma original durante el movimiento. También se procesaron modelos de superficie muscular para mostrar la deformación de la forma del músculo durante el movimiento. Los modelos de superficie de las articulaciones de las manos se movieron mediante el control virtual de las articulaciones. Guardamos 87 modelos de superficies móviles de la mano, incluidos huesos, músculos y ejes articulares en formato de estereolitografía, y compilamos un archivo en formato de documento portátil (PDF). Usando el archivo PDF, los movimientos de las articulaciones en una mano se pueden observar considerando los ejes X, Y y Z junto con las formas estereoscópicas de los huesos y músculos. Estos modelos de superficie móvil de la mano mejorarán la comprensión de los estudiantes de medicina sobre los movimientos de la mano alrededor de las articulaciones.

PALABRAS CLAVE: Articulaciones de las manos; Contracción muscular; Relajación muscular; Imágenes tridimensionales; Proyectos humanos visibles.

REFERENCES

Batmanabane, M. & Malathi, S. Movements at the carpometacarpal and metacarpophalangeal joints of the hand and their effect on the dimensions of the articular ends of the metacarpal bones. Anat. Rec., 213(1):102-10, 1985.

Glass, B. & Kistler, J. C. Distal hyperextensibility of the thumbs. Hum. Hered., 4(2-3):192-206, 1953.

Kim, C. Y.; Jung, Y. W. & Park, J. S. The Visible Korean: movable surface models of the hip joint. Surg. Radiol. Anat., 43(4):559-66, 2021a.

Kim, C. Y.; Lee, A. K.; Choi, H.D. & Park, J. S. Posture-transformed monkey phantoms developed from a Visible Monkey. Appl. Sci., 11(10):4430, 2021b.

Lewis, T.; Burnett, B.; Tunstall, R. & Abrahams, P. Complementing anatomy education using three-dimensional anatomy mobile software applications on tablet computers. Clin. Anat., 27(3):313-20, 2014.

Ling, Z. X. & Kumar, V. P. The myofascial compartments of the foot: a cadaver study. J. Bone Joint Surg. Br., 90(8):1114-8, 2008.

Moore, K. L.; Dalley, A. F. & Agur, A. M. R. Clinically Oriented Anatomy. 8th ed. Philadelphia, Wolters Kluwer, 2018a. pp.278-83.

Moore, K. L.; Dalley, A. F. & Agur, A. M. R. Clinically Oriented Anatomy. 8th ed. Philadelphia, Wolters Kluwer, 2018b. pp.27.

Onyije, F. M.; Oyinbo, C. A. & Waritimi, E. G. The prevalence and comparison of bent little finger and hitchhiker's thumb in South-South Nigeria. Eur. J. Appl. Sci., 4(4):157-9, 2012.

Park, J. S.; Chung, M. S.; Hwang, S. B.; Lee, Y. S.; Har, D. H. & Park, H. S. Visible Korean human: improved serially sectioned images of the entire body. IEEE Trans. Med. Imaging, 24(3):352-60, 2005.

Patel, S.; Potty, A.; Taylor, E. J. & Sorene, E. D. Collateral ligament injuries of the metacarpophalangeal joint of the thumb: a treatment algorithm. Strategies Trauma Limb Reconstr., 5(1):1-10, 2010.

Pazzaglia, U. E.; Sibilia, V.; Casati, L.; Salvi, A. G.; Minini, A. & Reguzzoni, M. The missing segment of the autopod 1st ray: new insights from a morphometric study of the human hand. J. Anat., 233(6):828-42, 2018.

Peters, D. Description and interpretation of interphalangeal lines in tetrapods. Ichnos, 7(1):11-41, 2000.

Shin, D. S.; Chung, M. S.; Park, J. S.; Park, H. S.; Lee, S.; Moon, Y. L. & Jang H. G. Portable document format file showing the surface models of cadaver whole body. J. Korean Med. Sci., 27(8):849-56, 2012a.

Shin, D. S.; Jang, H. G.; Park, J. S.; Park, H. S.; Lee, S. & Chung, M. S. Accessible and informative sectioned images and surface models of a cadaver head. J. Craniofac. Surg., 23(4):1176-80, 2012b.

Shin, D. S.; Park, J. S.; Park, H.S.; Hwang, S. B. & Chung, M. S. Outlining of the detailed structures in sectioned images from Visible Korean. Surg. Radiol. Anat., 34(3):235-47, 2012c.

Zilverschoon, M.; Kotte, E. M. G.; van, Esch. B.; Ten Cate, O.; Custers, E. J. & Bleys, R. L. A. W. Comparing the critical features of e-applications for three-dimensional anatomy education. Ann. Anat., 222:28-39, 2019.

Zilverschoon, M.; Vincken, K. L. & Bleys, R. L. A. W. The virtual dissecting room: Creating highly detailed anatomy models for educational purposes. J. Biomed. Inform., 65:58-75, 2017.

Corresponding author:
Jin Seo Park, Department of Anatomy
Dongguk University School of Medicine
87 Dongdae-ro
Gyeongju 38066
REPUBLIC OF KOREA

E-mail: park93@dongguk.ac.kr

Chung Yoh Kim (https://orcid.org/0000-0001-8074-076X)
JinSeo Park (https://orcid.org/0000-0001-7956-4148)